Analysis of Concentration Overpotential in an All-Vanadium Redox Flow Battery

Analysis of Concentration Overpotential in an All-Vanadium Redox Flow Battery

Sri Krishna Murthy,[1] Ashwini Kumar Sharma,[2,*,z] Clement Choo,[3] and Erik Birgersson[4]

[1]*Department of Chemical and Biomolecular Engineering, National University of Singapore, Singapore 117576*
[2]*Department of Chemical and Biochemical Engineering, Indian Institute of Technology Patna, India 801106*
[3]*Engineering Science Programme, National University of Singapore, Singapore 119077*
[4]*Department of Mechanical Engineering, National University of Singapore, Singapore 117575*

In electrochemical cells, transport of chemical species to/from the electrodes is limited by the mass transfer resistance between the electrode surface and the bulk electrolyte. This mass transfer resistance thus contributes to voltage losses, referred to as mass transport losses or concentration overpotential, compared to the reversible potential of cell. In this paper, we derived analytical expressions for estimating the mass transport losses in all-vanadium redox flow batteries. A step-by-step analysis allows us to relate the surface and bulk concentrations and then, identify the voltage losses due to mass transport from the Nernst equation and the Butler-Volmer kinetics. A zero-dimensional (0D) model with the derived expressions for the concentration overpotential is calibrated and validated with experimental data; good agreement is obtained. The mass transport losses from the Butler-Volmer kinetics are found to be approximately twice of that from the Nernst equation.

 [DOI: 10.1149/2.0681809jes]

Manuscript submitted February 19, 2018; revised manuscript received May 21, 2018. Published June 9, 2018.

An all-vanadium redox flow battery (VRFB) system comprises two electrolyte storage tanks in addition to an electrochemical stack. The latter facilitates charge transfer reactions at the constituent porous electrodes whereas the tanks store the energy in the form of electrolytes containing soluble redox couples (electroactive species). During charge and discharge, the electrolyte solutions are circulated through the electrodes where the electrochemical reactions take place. VRFB has shown great commercial prospects with its inherent characteristics, i.e., decoupled energy and power density, low maintenance, tolerance to deep charge and discharge, safer operations, longer cycle life, and energy efficiencies of up to 80% in large installations.[1] During charge, VO^{2+} at the positive electrode reacts to form VO_2^+ releasing electrons which flow through the external circuit and react with V^{3+} at the negative electrode to form V^{2+}. This process is reversible during discharge. The above reactions during charge and discharge operation of a VRFB can be summarized as follows:

$$V^{3+} + e^- \underset{\text{discharge}}{\overset{\text{charge}}{\rightleftharpoons}} V^{2+} \text{ at the negative electrode,} \quad [1]$$

$$VO^{2+} + H_2O \underset{\text{discharge}}{\overset{\text{charge}}{\rightleftharpoons}} VO_2^+ + e^- + 2H^+ \text{ at the positive electrode.} \quad [2]$$

The performance of a VRFB is affected by the reactant and product concentrations at the electrode surface as described in the Nernst equation and the Butler-Volmer (BV) equation. The former is used to evaluate the reversible electrode potential under non-standard conditions whereas the latter suggests the reaction kinetics at the electrodes, i.e., the functional relationship between the current produced by the electrochemical reaction and the activation losses occurring. From Fig. 1, it can be seen that the species are transported from the bulk to the electrode surface where the charge transfer kinetics takes place. A higher mass transport resistance could lead to reactant depletion and/or product accumulation at the electrode surface. Due to the dependence on concentrations, the performance of a VRFB will be adversely affected in turn. The loss in performance due to high mass transport resistance is referred to as the mass transport losses or concentration overpotential.

A number of mathematical models have been developed to study the role of mass transport resistance, i.e., concentration overpotential in VRFBs. Some of these models[2–19] include the mass transfer losses only for the reaction kinetics, given by the BV equation, whereas the other models[20–27] account for these losses only for evaluating the reversible electrode potential under non-standard conditions by the Nernst equation. As discussed above, the species concentrations effect both the reaction kinetics and the reversible electrode potentials. Thus, there are two different ways, the mass transfer resistance contributes to the voltage losses. The total concentration overpotential at an electrode is the sum of the two contributions. Further, the earlier studies,[20–26] to evaluate the mass transport losses, consider only the reactant depletion effects, not the product accumulation effects.

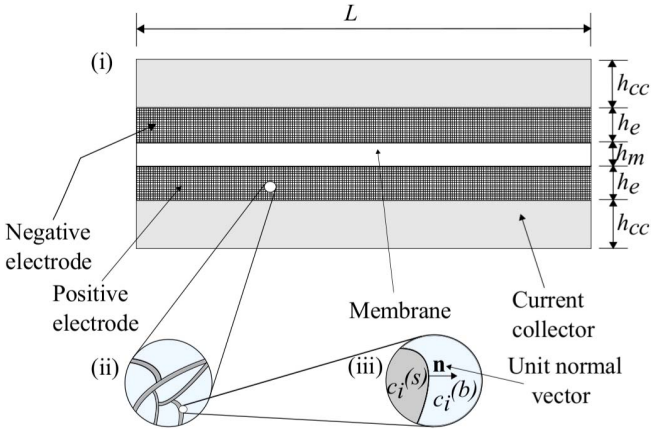

Figure 1. Schematic of transport of species in an electrode: (i) components of a VRFB, (ii) carbon fibers in a porous electrode, and (iii) transport of species in the carbon fibers.

The aim of the paper is two-fold: i) to show that the overpotential in the BV kinetics equation is the sum of the activation and the concentration overpotentials; and ii) to deduce the Nernst and the BV components of the concentration overpotential. First, we summarize a 0D mathematical model to evaluate the voltage of a VRFB. Further, we apply a mass balance over the boundary layer surrounding the carbon fibers to relate the surface and bulk concentrations of the vanadium ions taking into account the reactions occurring at the electrodes of the flow battery. Next, we discern the contribution of the Nernst equation and the BV kinetics toward concentration overpotential. Subsequently, we derive the expression for the cell voltage of a VRFB summarizing the analysis carried out. Finally, calibration and validation of the model with experimental data rounds up the paper.

Mathematical Formulation

Cell voltage.—In our previous work,[28] we reduced a three-dimensional (3D) of a flow battery to a 0D model using asymptotic

*Electrochemical Society Member.
[z]E-mail: ashwinikumar@iitp.ac.in; ashwini.ashwin@gmail.com

and scaling arguments. The 0D model for a single cell of VRFB is as follows:

$$E_{\text{cell}} = E^{\text{OCV}}(c) - \eta_{\text{neg}}(c, I) + \eta_{\text{pos}}(c, I) + I R_{\text{cell}}, \quad [3]$$

$$E^{\text{OCV}} = E_{\text{pos}} - E_{\text{neg}}, \quad [4]$$

$$E_{\text{pos}} = E^0_{\text{pos}} + \frac{RT}{F} \ln\left(\frac{c_{\text{VO}_2^+}}{c_{\text{VO}^{2+}}}\right), \quad [5]$$

$$E_{\text{neg}} = E^0_{\text{neg}} + \frac{RT}{F} \ln\left(\frac{c_{\text{V}^{3+}}}{c_{\text{V}^{2+}}}\right), \quad [6]$$

where I is the applied current ($I > 0$ during charge and $I < 0$ during discharge), R_{cell} is the total electronic resistance for ionic and electronic conduction in the cell, E is the reversible potential, E^0 is the standard reduction potential, R is the molar gas constant, F is the Faraday constant, c is the average concentration of the vanadium ions, η is the overpotential, T is the cell temperature; subscripts, pos and neg, denote the positive and the negative electrode respectively. The bulk concentration of the species, $c_i^{(\text{b})}$ are given by,[29]

$$c^{(\text{b})}_{\text{V}^{2+}} = c^{(\text{b})}_{\text{VO}_2^+} = c^0_{\text{V}^{2+}} + \frac{n_c I t}{V_{\text{tank}} F}, \quad [7]$$

$$c^{(\text{b})}_{\text{V}^{3+}} = c^{(\text{b})}_{\text{VO}^{2+}} = c^0_{\text{V}^{3+}} - \frac{n_c I t}{V_{\text{tank}} F}, \quad [8]$$

where $c^0_{\text{V}^{2+}}$ and $c^0_{\text{V}^{3+}}$ are initial concentration of V^{2+} and V^{3+} ions at the start of each charge and discharge cycle, and V_{tank} is the volume of the electrolyte tanks. Assuming that all the cells in the stack are identical in terms of both design and operating conditions, only a single cell is simulated and voltage of a single cell (E_{cell}) is multiplied by the number of cells (n_c) to obtain the stack voltage (E_{stack}):

$$E_{\text{stack}} = n_c E_{\text{cell}} \quad [9]$$

The assumption of extrapolating a single cell to describe the behavior of the whole stack has drawbacks as identified in Refs. 30,31. However, it allows for an efficient and tractable mathematical framework suitable for analysis and wide-ranging parametric studies, and therefore has been widely employed in modeling of bipolar electrochemical stacks.[30,32–34]

Bulk and surface concentrations.—To correlate bulk and surface concentration of the species, we write a mass balance over a boundary layer surrounding the carbon fibers yielding pointwise fluxes as in Fig. 1(iii). For the case of V^{3+} ions at the negative electrode, the mass balance is given by,

$$A_s\left(-D_{\text{V}^{3+}} \frac{\Delta c}{\delta}\right) = -\frac{I}{F}, \quad [10]$$

where $\Delta c = c^{(\text{b})}_{\text{V}^{3+}} - c^{(\text{s})}_{\text{V}^{3+}}$, and A_s is the local surface area; superscripts, (b) and (s) denote bulk and electrode surface respectively. Substituting the ratio of D_i and δ as the mass transfer coefficient (k_m), we get,

$$-k_m \Delta c = -\frac{I}{A_s F}, \quad [11]$$

$$\Delta c = \frac{I}{k_m a V_e F}, \quad [12]$$

where $A_s = aV_e$, a is the specific surface area of the electrode, and $V_e = w_{\text{cell}} L h_e$ is total volume (liquid and solid) of the electrode. Hence,

$$c^{(\text{s})}_{\text{V}^{3+}} = c^{(\text{b})}_{\text{V}^{3+}} - \Delta c. \quad [13]$$

Since $I > 0$ during charge, $\Delta c > 0$ (from Eq. 12). This infers that $c^{(\text{s})}_{\text{V}^{3+}} < c^{(\text{b})}_{\text{V}^{3+}}$ which is expected as V^{3+} ions are being consumed at the electrode surface during charge (see reaction at the negative electrode). In contrast, $\Delta c < 0$ and thus, $c^{(\text{s})}_{\text{V}^{3+}} > c^{(\text{b})}_{\text{V}^{3+}}$ during discharge ($I > 0$).

Similarly, we can write for V^{2+} ions at the negative electrode, and VO^{2+} and VO_2^+ ions at the positive electrode.

$$c^{(\text{s})}_{\text{V}^{2+}} = c^{(\text{b})}_{\text{V}^{2+}} + \Delta c \quad [14]$$

$$c^{(\text{s})}_{\text{VO}^{2+}} = c^{(\text{b})}_{\text{VO}^{2+}} - \Delta c \quad [15]$$

$$c^{(\text{s})}_{\text{VO}_2^+} = c^{(\text{b})}_{\text{VO}_2^+} + \Delta c \quad [16]$$

Mass transfer coefficient.—The mass transfer coefficient (k_m) is in general calibrated with the experiments.[35] For the carbon felt electrodes in VRFBs, k_m can be approximated by the following functional form:[36,37]

$$k_m = \mathfrak{a} u^{\mathfrak{b}}, \quad [17]$$

where u is the superficial velocity of the electrolyte flowing through the electrodes, $\mathfrak{a}$ and $\mathfrak{b}$ are fitted parameters. We determine $\mathfrak{a}$ and $\mathfrak{b}$ by fitting with the experiments.

Formal potentials.—While evaluating the reversible potential with the Nernst equation of the form in Eqs. 5–6, activity coefficients of the species are ignored, i.e., considered to be equal to unity. This is a common assumption employed in VRFB modeling. However, the assumption has limitations that were indeed confirmed in Refs. 38,39. In the above works, the open circuit voltages predicted by the Nernst equations with standard reduction potentials were observed to deviate from the experimentally measured OCVs. Pavelka et al.[38] further analyzed this deviation and revealed the limitations of ignoring the activity coefficients (equal to unity) in the Nernst equation. Thus, incorporating the activity coefficients in the Nernst equations is suggested.[38] An easy way to account for activity coefficients of the species in Nernst equation is to use the formal potential instead of the standard reduction potential.[40,41] In this work, we group the deviation between the formal and the standard reduction potential for the two electrodes in a single parameter, $\mathfrak{e}$ and thus, write

$$E^{\text{OCV}} = E_{\text{pos}} - E_{\text{neg}} + \mathfrak{e}, \quad [18]$$

Since the activity coefficients of ionic species are experimentally unavailable,[38,42] the formal potential or its deviation from the standard reduction potential (i.e., $\mathfrak{e}$ here) has to be tuned with the measurements.[38]

Analysis

Nernst potential.—Having correlated the bulk and surface concentration of the species, we analyze the Nernst equation to deduce the concentration overpotential component arising from it. When the mass transport of the species from the bulk to the surface or vice-versa is a limiting step in the overall electrochemical process, the equilibrium potential of the electrode is given by the Nernst equation of the form

$$E_{\text{neg}} = E^0_{\text{neg}} + \frac{RT}{F} \ln\left(\frac{c^{(\text{s})}_{\text{V}^{3+}}}{c^{(\text{s})}_{\text{V}^{2+}}}\right), \quad [19]$$

$$E_{\text{pos}} = E^0_{\text{pos}} + \frac{RT}{F} \ln\left(\frac{c^{(\text{s})}_{\text{VO}_2^+}}{c^{(\text{s})}_{\text{VO}^{2+}}}\right). \quad [20]$$

Based on the reactions taking place during charge and discharge, we can write after substituting surface concentrations,

$$E_{\text{neg}} = E^0_{\text{neg}} + \frac{RT}{F} \ln\left(\frac{c^{(\text{b})}_{\text{V}^{3+}} - \Delta c}{c^{(\text{b})}_{\text{V}^{2+}} + \Delta c}\right), \quad [21]$$

$$E_{pos} = E^0_{pos} + \frac{RT}{F}\ln\left(\frac{c^{(b)}_{VO_2^+} + \Delta c}{c^{(b)}_{VO^{2+}} - \Delta c}\right) \quad [22]$$

In order to distinguish bulk and surface concentrations, Eqs. 21 and 22 can be rearranged to give

$$E_{neg} = E^0_{neg} + \frac{RT}{F}\ln\left(\frac{c^{(b)}_{V^{3+}}}{c^{(b)}_{V^{2+}}}\right) + \frac{RT}{F}\ln\left(\frac{1 - \Delta c/c^{(b)}_{V^{3+}}}{1 + \Delta c/c^{(b)}_{V^{2+}}}\right), \quad [23]$$

$$E_{pos} = E^0_{pos} + \frac{RT}{F}\ln\left(\frac{c^{(b)}_{VO_2^+}}{c^{(b)}_{VO^{2+}}}\right) + \frac{RT}{F}\ln\left(\frac{1 + \Delta c/c^{(b)}_{VO_2^+}}{1 - \Delta c/c^{(b)}_{VO^{2+}}}\right). \quad [24]$$

The first two terms in the expression for E_{neg} and E_{pos} respectively constitute the Nernst equation with bulk concentrations for the negative and positive electrode (Eqs. 5–6). They are applicable as it is in the case of negligible mass transfer resistance ($k_m \to \infty$ or $\Delta c \approx 0$), i.e., when the rate of transfer of species is fast enough compared to the rate of consumption or production of the ions. The remaining two terms in Eqs. 23 and 24 are correction terms for a significant mass transfer resistance, i.e., on employing the surface concentrations instead of bulk concentrations and therefore, represent the voltage losses due to mass transport resistance at the surface of the electrodes. We can write expressions for such voltage losses, i.e., concentration overpotential from the Nernst equation for the two electrodes as follows

$$\eta^{conc}_{neg,Nernst} = \frac{RT}{F}\ln\left(\frac{1 - \Delta c/c^{(b)}_{V^{3+}}}{1 + \Delta c/c^{(b)}_{V^{2+}}}\right), \quad [25]$$

$$\eta^{conc}_{pos,Nernst} = \frac{RT}{F}\ln\left(\frac{1 + \Delta c/c^{(b)}_{VO_2^+}}{1 - \Delta c/c^{(b)}_{VO^{2+}}}\right). \quad [26]$$

Reaction kinetics.—In this subsection, we aim to deduce the concentration overpotential component arising from the BV equation and also show that the overpotential is the sum of the activation and concentration overpotentials. To do so, we consider the generalized BV equation which incorporates the mass transport resistance of the species while accounting for the reaction kinetics at the electrodes in the VRFB.[2,4–6,8]

$$J_{neg} = ai^0_{neg}\left\{\frac{c^{(s)}_{V^{2+}}}{c^{(b)}_{V^{2+}}}\exp\left[\frac{(1-\alpha_{neg})F\eta_{neg}}{RT}\right] - \frac{c^{(s)}_{V^{3+}}}{c^{(b)}_{V^{3+}}}\exp\left[-\frac{\alpha_{neg}F\eta_{neg}}{RT}\right]\right\}, \quad [27]$$

$$J_{pos} = ai^0_{pos}\left\{\frac{c^{(s)}_{VO^{2+}}}{c^{(b)}_{VO^{2+}}}\exp\left[\frac{(1-\alpha_{pos})F\eta_{neg}}{RT}\right] - \frac{c^{(s)}_{VO_2^+}}{c^{(b)}_{VO_2^+}}\exp\left[-\frac{\alpha_{pos}F\eta_{neg}}{RT}\right]\right\}, \quad [28]$$

where η represents the total voltage losses for an electrochemical reaction taking place, i.e., it incorporates the voltage losses to overcome the activation barrier (activation overpotential) as well as the mass transport resistance (concentration overpotential), and

$$i^0_{neg} = Fk_{neg}\left(c^{(b)}_{V^{2+}}\right)^{(1-\alpha_{neg})}\left(c^{(b)}_{V^{3+}}\right)^{\alpha_{neg}}, \quad [29]$$

$$i^0_{pos} = Fk_{pos}\left(c^{(b)}_{VO^{2+}}\right)^{(1-\alpha_{pos})}\left(c^{(b)}_{VO_2^+}\right)^{\alpha_{pos}}, \quad [30]$$

where α_{neg} and α_{pos} are the charge transfer coefficients for negative and positive electrode respectively, and k_{neg} and k_{pos} are the reaction rate constants for negative and positive electrode respectively.

When there is negligible mass transfer resistance, i.e. $c^{(b)} \approx c^{(s)}$, the voltage losses at the electrodes are purely due to charge transfer resistance. For such a case, Eqs. 27 and 28 reduce to

$$J_{neg} = ai^0_{neg}\left[\exp\left(\frac{(1-\alpha_{neg})F\eta^{act}_{neg}}{RT}\right) - \exp\left(-\frac{\alpha_{neg}F\eta^{act}_{neg}}{RT}\right)\right], \quad [31]$$

$$J_{pos} = ai^0_{pos}\left[\exp\left(\frac{(1-\alpha_{pos})F\eta^{act}_{pos}}{RT}\right) - \exp\left(-\frac{\alpha_{pos}F\eta^{act}_{pos}}{RT}\right)\right]. \quad [32]$$

Substituting $J_{pos} = \frac{I}{V_e}$, $J_{neg} = -\frac{I}{V_e}$, and symmetric charge transfer ($\alpha = 0.5$), the expression for η^{act} in Eqs. 31 and 32 becomes,

$$\eta^{act}_{neg} = -\frac{2RT}{F}\sinh^{-1}\left(\frac{I}{2aFV_e k_{neg}\sqrt{c^{(b)}_{V^{2+}}c^{(b)}_{V^{3+}}}}\right), \quad [33]$$

$$\eta^{act}_{pos} = \frac{2RT}{F}\sinh^{-1}\left(\frac{I}{2aFV_e k_{pos}\sqrt{c^{(b)}_{VO^{2+}}c^{(b)}_{VO_2^+}}}\right). \quad [34]$$

The above two terms represent the voltage losses to overcome the activation barrier and therefore, are referred to as the activation overpotentials.

Next, we proceed to pull out the concentration overpotential terms inherent in the Bulter-Volmer equations (Eqs. 27–28). The concentration losses are most pronounced at higher current densities where one term in the BV equation is typically much larger than the other. The relative magnitude of the two terms depends on the electrode and charge/discharge. For example, the second term dominates for the negative electrode (Eq. 27) during charging and thus, the BV equation is simplified to

$$J_{neg} = -ai^0_{neg}\left[\frac{c^{(s)}_{V^{3+}}}{c^{(b)}_{V^{3+}}}\exp\left(\frac{-F\eta_{neg}}{2RT}\right)\right], \quad [35]$$

After substituting surface concentration in terms of bulk concentration, Eq. 35 becomes

$$\eta_{neg} = -\frac{2RT}{F}\ln\left[\frac{-J_{neg}}{ai^0_{neg}}\frac{c^{(b)}_{V^{3+}}}{c^{(b)}_{V^{3+}} - \Delta c}\right], \quad [36]$$

$$= -\frac{2RT}{F}\ln\left[\frac{-J_{neg}}{ai^0_{neg}}\right] - \frac{2RT}{F}\ln\left[\frac{c^{(b)}_{V^{3+}}}{c^{(b)}_{V^{3+}} - \Delta c}\right]. \quad [37]$$

The first term is a simplified expression of the activation overpotential at higher current densities. This is identified by substituting $\Delta c \approx 0$ in Eq. 36 which corresponds to a negligible mass transfer resistance ($k_m \to \infty$). Note that we shall continue to use expressions in Eqs. 33, 34 for estimation of the activation overpotentials. The second term in Eq. 37 accounts for the losses associated with the mass transport resistance between the bulk and surface of the electrodes:

$$\eta^{conc}_{neg,BV} = -\frac{2RT}{F}\ln\left[\frac{c^{(b)}_{V^{3+}}}{c^{(b)}_{V^{3+}} - \Delta c}\right]. \quad [38]$$

During discharging, the first term dominates for the negative electrode (Eq. 27) whence the BV equation is simplified to

$$J_{neg} = ai^0_{neg}\left[\frac{c^{(s)}_{V^{2+}}}{c^{(b)}_{V^{2+}}}\exp\left(\frac{F\eta_{neg}}{2RT}\right)\right], \quad [39]$$

Again, substituting surface concentration in terms of bulk concentration, the term describing the mass transport losses can be identified as

follows:

$$\eta^{\text{conc}}_{\text{neg,BV}} = \frac{2RT}{F} \ln\left[\frac{c^{(\text{b})}_{\text{V}^{2+}}}{c^{(\text{b})}_{\text{V}^{2+}} + \Delta c}\right]. \quad [40]$$

Similarly, the mass transport losses contained in the kinetics expression for the positive electrode during charge are written as follows

$$\eta^{\text{conc}}_{\text{pos,BV}} = \frac{2RT}{F} \ln\left[\frac{c^{(\text{b})}_{\text{VO}^{2+}}}{c^{(\text{b})}_{\text{VO}^{2+}} - \Delta c}\right], \quad [41]$$

and during discharge, they become

$$\eta^{\text{conc}}_{\text{pos,BV}} = -\frac{2RT}{F} \ln\left[\frac{c^{(\text{b})}_{\text{VO}_2^+}}{c^{(\text{b})}_{\text{VO}_2^+} + \Delta c}\right]. \quad [42]$$

The generalized expression for the BV component of the concentration overpotential at the negative electrode can be written as,

$$\eta^{\text{conc}}_{\text{neg,BV}} = \mp\frac{2RT}{F} \ln\left[\frac{c^{(\text{b})}_{i}}{c^{(\text{b})}_{i} - |\Delta c|}\right], \quad [43]$$

During charging, the negative sign holds and species i represents V^{3+} whereas the positive sign holds and species i represents V^{2+} during discharging.

Similarly, the generalized expression for the BV component of the concentration overpotential at the positive electrode can be written as,

$$\eta^{\text{conc}}_{\text{pos,BV}} = \mp\frac{2RT}{F} \ln\left[\frac{c^{(\text{b})}_{i} - |\Delta c|}{c^{(\text{b})}_{i}}\right], \quad [44]$$

During charging, the negative sign holds and species i represents VO^{2+} whereas the positive sign holds and species i represents VO_2^+ during discharging.

Results

Cell voltage.—In the preceding section, we have deduced the concentration overpotential components from both the Nernst and BV equation. Thus, the equation for cell voltage prediction (Eq. 3) becomes (N.B.: we refer to earlier sections for nomenclature of symbols):

$$E_{\text{cell}} = E^{\text{OCV}}(c^{(\text{b})}) - \eta^{\text{act}}_{\text{neg}}(c^{(\text{b})}, I) - \eta^{\text{conc}}_{\text{neg}}(c^{(\text{b})}, I) + \eta^{\text{act}}_{\text{pos}}(c^{(\text{b})}, I) + \eta^{\text{conc}}_{\text{pos}}(c^{(\text{b})}, I) + I R_{\text{cell}}, \quad [45]$$

$$E^{\text{OCV}} = E_{\text{pos}} - E_{\text{neg}} + \mathfrak{e}, \quad [46]$$

$$E_{\text{pos}} = E^{0}_{\text{pos}} + \frac{RT}{F} \ln\left(\frac{c^{(\text{b})}_{\text{VO}_2^+}}{c^{(\text{b})}_{\text{VO}^{2+}}}\right), \quad [47]$$

$$E_{\text{neg}} = E^{0}_{\text{neg}} + \frac{RT}{F} \ln\left(\frac{c^{(\text{b})}_{\text{V}^{3+}}}{c^{(\text{b})}_{\text{V}^{2+}}}\right), \quad [48]$$

$$\eta^{\text{act}}_{\text{neg}} = -\frac{2RT}{F} \sinh^{-1}\left(\frac{I}{2aFV_e k_{\text{neg}}\sqrt{c^{(\text{b})}_{\text{V}^{2+}} c^{(\text{b})}_{\text{V}^{3+}}}}\right), \quad [49]$$

$$\eta^{\text{act}}_{\text{pos}} = \frac{2RT}{F} \sinh^{-1}\left(\frac{I}{2aFV_e k_{\text{pos}}\sqrt{c^{(\text{b})}_{\text{VO}^{2+}} c^{(\text{b})}_{\text{VO}_2^+}}}\right), \quad [50]$$

Table I. Operating and physical parameters.[43]

Parameter	Value	Units
L	0.35	m
w_{cell}	0.25	m
h_{e}	4	mm
a	2×10^5	m^{-1}
N_{c}	15	-
T	300	K
V_{tank}	20	L
$c^0_{\text{V}^{3+}}$	1499	mol m^{-3}
$c^0_{\text{V}^{2+}}$	1	mol m^{-3}
$c^0_{\text{VO}^{2+}}$	1499	mol m^{-3}
$c^0_{\text{VO}_2^+}$	1	mol m^{-3}
$\dot{V}$	0.2, 0.71	$\text{m}^3\ \text{h}^{-1}$
i_{app}	45, 75	mA cm^{-2}
$E_{0,\text{pos}}$	1.004	V
$E_{0,\text{neg}}$	−0.255	V
R	8.314	$\text{J mol}^{-1}\ \text{K}^{-1}$
F	96500	A s mol^{-1}
R_{cell}	2.2	mΩ

$$\eta^{\text{conc}}_{\text{neg}} = \eta^{\text{conc}}_{\text{neg,Nernst}} + \eta^{\text{conc}}_{\text{neg,BV}}, \quad [51]$$

$$\eta^{\text{conc}}_{\text{pos}} = \eta^{\text{conc}}_{\text{pos,Nernst}} + \eta^{\text{conc}}_{\text{pos,BV}}, \quad [52]$$

$$\eta^{\text{conc}}_{\text{neg,BV}} = \mp\frac{2RT}{F} \ln\left[\frac{c^{(\text{b})}_{i}}{c^{(\text{b})}_{i} - |\Delta c|}\right], \quad [53]$$

$$\eta^{\text{conc}}_{\text{pos,BV}} = \mp\frac{2RT}{F} \ln\left[\frac{c^{(\text{b})}_{i} - |\Delta c|}{c^{(\text{b})}_{i}}\right], \quad [54]$$

$$\eta^{\text{conc}}_{\text{neg,Nernst}} = \frac{RT}{F} \ln\left(\frac{1 - \Delta c/c^{(\text{b})}_{\text{V}^{3+}}}{1 + \Delta c/c^{(\text{b})}_{\text{V}^{2+}}}\right), \quad [55]$$

$$\eta^{\text{conc}}_{\text{pos,Nernst}} = \frac{RT}{F} \ln\left(\frac{1 + \Delta c/c^{(\text{b})}_{\text{VO}_2^+}}{1 - \Delta c/c^{(\text{b})}_{\text{VO}^{2+}}}\right), \quad [56]$$

When there is no mass transport resistance, i.e., $\Delta c = 0$, the concentration overpotential at both the electrodes (given by Eqs. 51 and 52) is zero and we have the following equation for cell voltage:

$$E_{\text{cell}} = E^{\text{OCV}}(c^{(\text{b})}) - \eta^{\text{act}}_{\text{neg}}(c^{(\text{b})}, I) + \eta^{\text{act}}_{\text{pos}}(c^{(\text{b})}, I) + I R_{\text{cell}} \quad [57]$$

This equation is widely used to predict cell voltage of a VRFB cell; however, this does not account for the concentration overpotential at both the electrodes and thus could lead to erroneous model predictions as discussed in the next section.

Calibration and validation.—We have thus far derived analytical expression for estimating the concentration overpotential in VRFBs and incorporated it in a 0D model. For numerical computation, this model is implemented on *MATLAB R2015a.*

In order to determine the unknown model parameters (k_{neg}, k_{pos}, $\mathfrak{a}$, $\mathfrak{b}$, and $\mathfrak{e}$) and verify the fidelity of the derived expression, we calibrate and validate the resulting 0D model with experimental data from Ma et al.[43] Table I summarizes the operating and physical parameters set in their experiments; the derived model is simulated for these values here. The above work reported a wide range of experimental measurements for varying current densities and flow rates. The latter

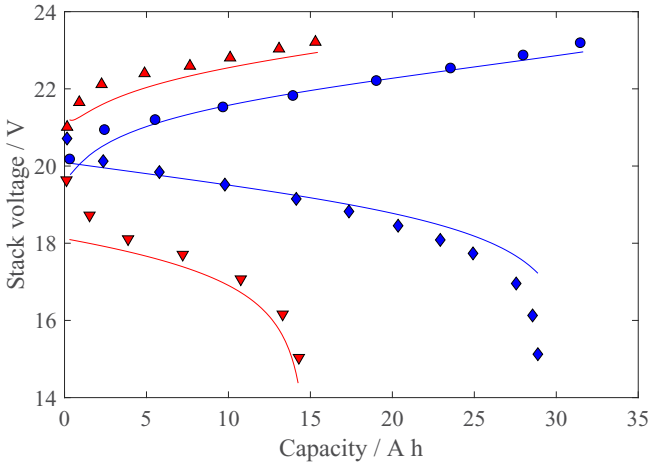

Figure 2. Charge discharge curves for a VRFB system: experiments (symbols)[43] and corresponding model predictions (lines) for a flow rate of 0.2 $m^3\ h^{-1}$; 45 mA cm^{-2}: charge (●) and discharge (◆); 75 mA cm^{-2}: charge (▲) and discharge (▼).

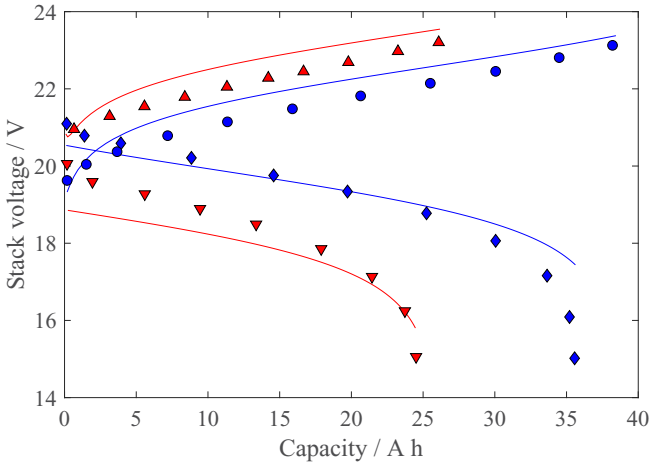

Figure 3. Charge discharge curves for a VRFB system: experiments (symbols)[43] and corresponding model predictions (lines) for a flow rate of 0.71 $m^3\ h^{-1}$; 45 mA cm^{-2}: charge (●) and discharge (◆); 75 mA cm^{-2}: charge (▲) and discharge (▼).

is of particular interest as the mass transfer coefficient (k_m) varies with the flow rates mainly.[38,39] The model is then calibrated for the unknown parameters with the help of charge-discharge measurements. Two different sets of data are generally used for model calibration and validation, referred to as the training and test sets. Here, we classify the charge-discharge measurements at 45 mA cm^{-2} for a flow rate of 0.2 $m^3\ h^{-1}$ as the training set and the remaining measurements at 45 and 75 mA cm^{-2} as the test set. Comparing model predictions and experimental voltages for the training set using the nonlinear least-squares method, the model is calibrated to determine the unknown model parameters:

$$k_{neg} = 7.9 \times 10^{-8}\ m\ s^{-1}, \quad [58]$$

$$k_{pos} = 6.4 \times 10^{-8}\ m\ s^{-1}, \quad [59]$$

$$\mathfrak{a} = 10^{-4}(m\ s^{-1})^{0.1}, \quad [60]$$

$$\mathfrak{b} = 0.9, \quad [61]$$

$$\mathfrak{e} = 155\ mV, \quad [62]$$

Note that the reaction rate constants for both the electrodes (k_{neg} and k_{pos}) are reported to be of the same order of magnitude in the earlier modeling studies.[2–27] Similarly, the prefactor ($\mathfrak{a}$) and the exponent ($\mathfrak{b}$) in the empirical correlation for mass transfer coefficient are also found to be in the range reported earlier for carbon felt electrodes.[36,37] Further, the deviation between the formal and standard reduction potential for a VRFB cell has also been found to be comparable with earlier reports.[38,39,41] Subsequently, to confirm the reliability of the calibrated model, the voltage profiles predicted by the model are compared with the test set for another flow rate of 0.71 m^3h^{-1} at 45 mA cm^{-2} and another current density of 75 mA cm^{-2}at 0.2 and 0.71 m^3h^{-1}. Good agreement is obtained as shown in Figs. 2–3 with an average relative error of ∼5% for all charge-discharge cycles.

The open circuit voltage of a VRFB cell is a function of vanadium species concentrations (Eqs. 46–48). Thus, it changes continuously during both charge and discharge of the cell (see Fig. 4). Initially, there is only one ionic species at each of the electrodes – V^{3+} at the negative and VO^{2+} at the positive electrode – whence there is a relatively large change in OCV against a small change in concentrations. This results into a non-linear increase in the stack voltage at the beginning of charge as observed in Figs. 2–3. Here, charging is

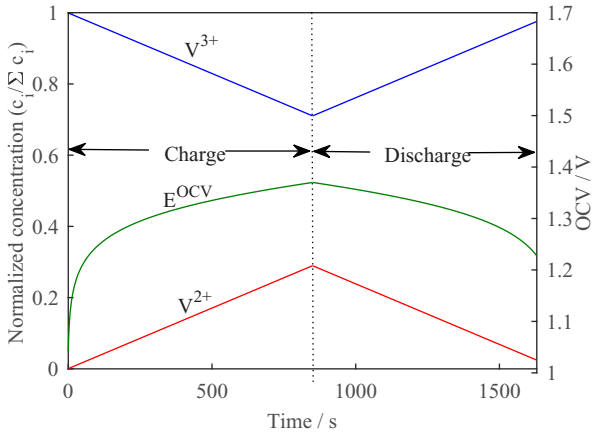

Figure 4. Evolution of species concentrations (at negative electrode) and open circuit voltage of a cell during a charge-discharge cycle at current density of 75 mA cm^{-2} and electrolyte flow rate of 0.2 $m^3\ h^{-1}$.

terminated after reaching a certain voltage. In this voltage range, both the vanadium species at each electrode are found to be in moderate concentrations (see Fig. 4) whence the stack voltage changes almost linearly at the end of charge and at the beginning of discharge. At the end of discharge, the reactant species at both the electrodes tends to their lower concentrations (see Fig. 4). This in conjunction with the mass transport effects results in sharp fall in stack voltage at the end of discharge (see Figs. 2–3).

To highlight the mass transport effects on voltage predictions, we proceed to compare the simulated voltage profiles with and without inclusion of different mass transport effects. For this purpose, let us consider the discharge operation of the flow battery at an applied current density of 75 mA cm^{-2} and an electrolyte flow rate of 0.2 $m^3\ h^{-1}$. When no mass transport effects are accounted for, all terms of the concentration overpotential can be dropped from the voltage equation (Eq. 45). With such a model, the fall in stack voltage toward the end of discharge is less steep as compared to the case when all these terms (mass transfer effects) are considered as shown in Fig. 5. Quantitatively, there is a relative difference of ∼10% in voltage predictions toward the end of discharge. Similarly, there are relative differences of ∼6% and ∼3% in predictions respectively when the mass transport effects on only the reversible potential (with the Nernst equation) and only on the reaction kinetics (with the BV equation) are accounted for. Thus, we can infer that the contribution of the BV equation

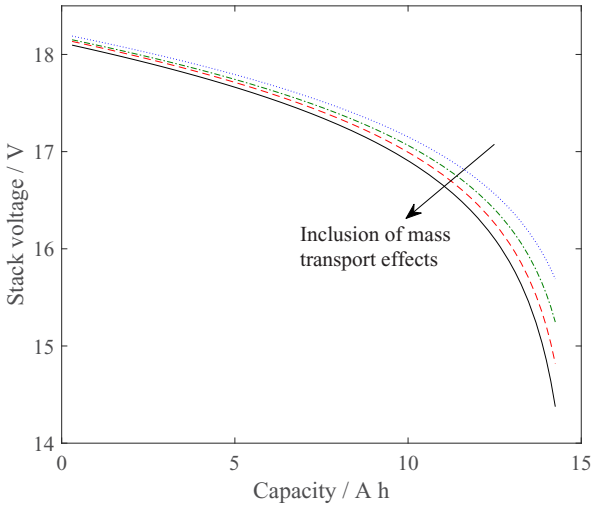

Figure 5. Discharge stack voltage predictions at current density of 75 mA cm^{-2} and and electrolyte flow rate of 0.2 m^3 h^{-1}: Model without any mass transport effects or concentration overpotential (dotted line), mass transport effects only on the reversible potential included (dashed-dotted line), mass transport effects only on the kinetics included (dashed line), mass transport effects on both the reversible potential and kinetics included (solid line).

toward the concentration overpotential in VRFB is almost twice that of the Nernst equation. The relative magnitude of the two types of contributions can be discerned from their mathematical expressions also (Eqs. 53–55). Since the logarithmic terms in the two expressions are of the same order of magnitude, the contribution of the BV equation is approximately twice that of the Nernst equation toward the concentration overpotential.

Conclusions

In this paper, we analyzed the mass transport losses, also referred to as the concentration overpotential in VRFBs. The analysis, in essence, relates the bulk and surface concentration of species and subsequently, finds the mass transport losses associated with the Nernst and BV equation. It is shown with the mass transfer coefficient approach that the surface concentration of a species is sum of its bulk concentration and a term (Δc_i) comprising operating conditions (I, v), and electrode and material properties (a). By employing this correlation in a 0D model framework, we discern the inherent overpotential components in a VRFB. The employed model is then calibrated and validated with the experimental data; good agreement is obtained. The mass transport losses are found to contribute significantly toward the end of charge and discharge of VRFBs, and therefore, are suggested to be treated separately in their performance analysis.

In short, the above analysis serves to comprehensively understand and quantify how the mass transfer resistance influences performance of a VRFB. The comprehensiveness is imparted by considering both the reactant depletion and product accumulation effects and accounting them in both the Nernst potential and reaction kinetics. The analysis is generic pertaining to the fact that similar mathematical equations are used to describe the transport phenomena in other flow batteries. Hence, it can easily be extended to other redox flow chemistries.

The 0D model adapted in this work provides an efficient tool for investigating VRFB operation, in particular the mass transfer effects. However, it is based on some assumptions, e.g., lumped parameter modeling (0D model), empirical mass transfer correlations, isothermal operation, etc. and therefore, has some restrictions as reported in Ref. 44. In this regard, we particularly note that the 0D formulation would inhibit the model to capture the effects of residence time in the cell. The comprehensive mass transfer effects identified in the analysis here can also be incorporated in detailed models and more accurate predictions could be achieved.

Acknowledgments

This research is supported by the National Research Foundation, Singapore under its Competitive Research Program (Award No. NRF-CRP8-2011-04). The authors would also like to acknowledge the support of National University of Singapore. The second author acknowledges the support of Indian Institute of Technology Patna. In addition, the authors thank the referees for their helpful comments on an earlier version of the article.

ORCID

Ashwini Kumar Sharma https://orcid.org/0000-0003-0329-3542

References

1. M. Skyllas-Kazacos and R. Robins, All-vanadium redox flow battery, U. S. patent, 4,786,567 (1988).
2. K. W. Knehr, E. Agar, C. R. Dennison, A. R. Kalidindi, and E. C. Kumbur, A transient vanadium flow battery model incorporating vanadium crossover and water transport through the membrane, *Journal of The Electrochemical Society*, **159**(9), A1446 (2012).
3. I. M. Bayanov and R. Vanhaelst, The numerical simulation of vanadium redox flow batteries, *Journal of mathematical chemistry*, **49**(9), 2013 (2011).
4. X. Ma, H. Zhang, and F. Xing, A three-dimensional model for negative half cell of the vanadium redox flow battery, *Electrochimica Acta*, **58**, 238 (2011).
5. K. Oh, H. Yoo, J. Ko, S. Won, and H. Ju, Three-dimensional, transient, nonisothermal model of all-vanadium redox flow batteries, *Energy*, **81**, 3 (2015).
6. D. You, H. Zhang, and J. Chen, A simple model for the vanadium redox battery, *Electrochimica Acta*, **54**(27), 6827 (2009).
7. X. L. Zhou, T. S. Zhao, L. An, Y. K. Zeng, and X. H. Yan, A vanadium redox flow battery model incorporating the effect of ion concentrations on ion mobility, *Applied Energy*, **158**, 157 (2015).
8. X. L. Zhou, T. S. Zhao, L. An, Y. K. Zeng, and L. Wei, Modeling of ion transport through a porous separator in vanadium redox flow batteries, *Journal of Power Sources*, **327**, 67 (2016).
9. A. A. Shah, M. J. Watt-Smith, and F. C. Walsh, A dynamic performance model for redox-flow batteries involving soluble species, *Electrochimica Acta*, **53**(27), 8087 (2008).
10. H. Al-Fetlawi, A. A. Shah, and F. C. Walsh, Non-isothermal modeling of the all-vanadium redox flow battery, *Electrochimica Acta*, **55**(1), 78 (2009).
11. H. Al-Fetlawi, A. A. Shah, and F. C. Walsh, Modelling the effects of oxygen evolution in the all-vanadium redox flow battery, *Electrochimica Acta*, **55**(9), 3192 (2010).
12. K. Bromberger, J. Kaunert, and T. Smolinka, A model for all-vanadium redox flow batteries: Introducing electrode-compression effects on voltage losses and hydraulics, *Energy Technology*, **2**(1), 64 (2014).
13. F. T. Wandschneider, D. Finke, S. Grosjean, P. Fischer, K. Pinkwart, J. Tübke, and H. Nirschl, Model of a vanadium redox flow battery with an anion exchange membrane and a larminie-correction, *Journal of Power Sources*, **272**, 436 (2014).
14. S. Won, K. Oh, and H. Ju, Numerical studies of carbon paper-based vanadium redox flow batteries, *Electrochimica Acta*, **201**, 286 (2016).
15. Y. Lei, B. W. Zhang, B. F. Bai, and T. S. Zhao, A transient electrochemical model incorporating the donnan effect for all-vanadium redox flow batteries, *Journal of Power Sources*, **299**, 202 (2015).
16. K. Oh, S. Won, and H. Ju, A comparative study of species migration and diffusion mechanisms in all-vanadium redox flow batteries, *Electrochimica Acta*, **181**, 238 (2015).
17. Y. Wang and S. C. Cho, Analysis and three-dimensional modeling of vanadium flow batteries, *Journal of The Electrochemical Society*, **161**(9), A1200 (2014).
18. Q. Xu, T. S. Zhao, and P. K. Leung, Numerical investigations of flow field designs for vanadium redox flow batteries, *Applied energy*, **105**, 47 (2013).
19. A. A. Shah, H. Al-Fetlawi, and F. C. Walsh, Dynamic modeling of hydrogen evolution effects in the all-vanadium redox flow battery, *Electrochimica Acta*, **55**(3), 1125 (2010).
20. Q. Ye, J. Hu, P. Cheng, and Z. Ma, Design trade-offs among shunt current, pumping loss and compactness in the piping system of a multi-stack vanadium flow battery, *Journal of Power Sources*, **296**, 352 (2015).
21. A. Tang, J. Bao, and M. Skyllas-Kazacos, Studies on pressure losses and flow rate optimization in vanadium redox flow battery, *Journal of power sources*, **248**, 154 (2014).
22. Y. Li, M. Skyllas-Kazacos, and J. Bao, A dynamic plug flow reactor model for a vanadium redox flow battery cell, *Journal of Power Sources*, **311**, 57 (2016).
23. Y. Li, X. Zhang, J. Bao, and M. Skyllas-Kazacos, Studies on optimal charging conditions for vanadium redox flow batteries, *Journal of Energy Storage*, **11**, 191 (2017).
24. Q. Zheng, F. Xing, X. Li, G. Ning, and H. Zhang, Flow field design and optimization based on the mass transport polarization regulation in a flow-through type vanadium flow battery, *Journal of Power Sources*, **324**, 402 (2016).

25. S. König, M. Suriyah, and T. Leibfried, Innovative model-based flow rate optimization for vanadium redox flow batteries, *Journal of Power Sources*, **333**, 134 (2016).
26. S. König, M. Suriyah, and T. Leibfried, A plug flow reactor model of a vanadium redox flow battery considering the conductive current collectors, *Journal of Power Sources*, **360**, 221 (2017).
27. S. König, M. Suriyah, and T. Leibfried, Validating and improving a zero-dimensional stack voltage model of the vanadium redox flow battery, *Journal of Power Sources*, **378**, 10 (2018).
28. A. K. Sharma, C. Y. Ling, E. Birgersson, M. Vynnycky, and M. Han, Verified reduction of dimensionality for an all-vanadium redox flow battery model, *Journal of Power Sources*, **279**, 345 (2015).
29. A. Tang, J. Bao, and M. Skyllas-Kazacos, Dynamic modeling of the effects of ion diffusion and side reactions on the capacity loss for vanadium redox flow battery, *Journal of Power Sources*, **196**(24), 10737 (2011).
30. I. B. Celik and S. R. Pakalapati, From a Single Cell to a Stack Modeling. In: R. Bove and S . bertini (eds) Modeling Solid Oxide Fuel Cells, Springer, Dordrecht (2008).
31. A. K. Sharma and E. Birgersson, Computationally-Efficient Simulation of Transport Phenomena in Fuel Cell Stacks via Electrical and Thermal Decoupling of the Cells, *Fuel Cells*, **14**(6), 906 (2014).
32. M. Duerr, S. Gair, A. Cruden, and J. McDonald, Dynamic electrochemical model of an alkaline fuel cell stack, *Journal of Power Sources*, **171**, 1023 (2007).
33. S. P. Philipps and C. Ziegler, Computationally efficient modeling of the dynamic behavior of a portable PEM fuel cell stack, *Journal of Power Sources*, **180**, 309 (2008).
34. Xiao-guang Li, Liu-lin Cao, Zhi-xiang Liu, and Cheng Wang, Development of a fast empirical design model for PEM stacks, *International Journal of Hydrogen Energy*, **35**, 2698 (2010).
35. R. E. Treybal, *Mass transfer operations*, McGraw-Hill chemical engineering series (1980).
36. X. You, Q. Ye, and P. Cheng, The dependence of mass transfer coefficient on the electrolyte velocity in carbon felt electrodes: determination and validation, *Journal of The Electrochemical Society*, **164**(11), E3386 (2017).
37. D. Schmal, J. Van Erkel, and P. J. Van Duin, Mass transfer at carbon fiber electrodes, *Journal of applied electrochemistry*, **16**(3), 422 (1986).
38. M. Pavelka, F. Wandschneider, and P. Mazur, Thermodynamic derivation of open circuit voltage in vanadium redox flow batteries, *Journal of Power Sources*, **293**, 400 (2015).
39. K. W. Knehr and E. C. Kumbur, Open circuit voltage of vanadium redox flow batteries: Discrepancy between models and experiments, *Electrochemistry Communications*, **13**(4), 342 (2011).
40. Cynthia G. Zoski, *Handbook of Electrochemistry*, Elsevier (2007).
41. S. Corcuera and M. Skyllas-Kazacos, State-of-charge monitoring and electrolyte rebalancing methods for the vanadium redox flow battery, *European Chemical Bulletin*, **1**(12), 511 (2012).
42. E. A. Guggenheim, The conceptions of electrical potential difference between two phases and the individual activities of ions, *The Journal of Physical Chemistry*, **33**(6), 842 (1929).
43. X. Ma, H. Zhang, C. Sun, Y. Zou, and T. Zhang, An optimal strategy of electrolyte flow rate for vanadium redox flow battery, *Journal of power sources*, **203**, 153 (2012).
44. Philipp A. Boettcher, Ertan Agar, C. R. Dennison, and E. Caglan Kumbur, Modeling of ion crossover in vanadium redox flow batteries: a computationally-efficient lumped parameter approach for extended cycling, *Journal of The Electrochemical Society*, **163**, A5244 (2016).